

# Facile Fabrication of Highly Stretchable, Stable, and Self-Healing Ion-Conductive Sensors for Monitoring Human Motions

Xiaohui Yu, Yong Zheng, Yufei Wang, Haopeng Zhang, Hui Song, Zibiao Li, Xiaoshan Fan,\* and Tianxi Liu\*



Cite This: *Chem. Mater.* 2022, 34, 1110–1120



Read Online

ACCESS |



Metrics & More

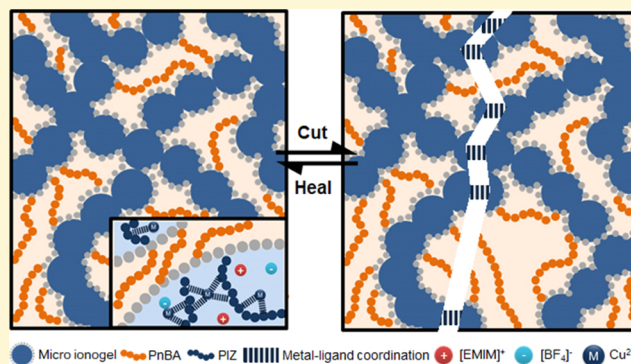


Article Recommendations



Supporting Information

**ABSTRACT:** Ionic liquid (IL)-based conductive elastomers have recently emerged as promising stretchable electrodes for applications in flexible electronic devices because of the interesting features of ILs. However, conventional IL-based elastomers suffer from low mechanical properties, instability in the ambient environment, and lack of self-healability. Herein, highly stretchable, stable, and self-healable IL-based conductive elastomers PnBA/SiO<sub>2</sub>/PVI (Cu<sup>2+</sup>, [EMIM]<sup>+</sup>[BF<sub>4</sub>]<sup>-</sup>) were designed and facilely fabricated by one-pot Pickering emulsion polymerization. The Pickering emulsion is composed of the continuous phase of *n*-butyl acrylate, the dispersed phase containing vinylimidazole, copper acetate and IL ([EMIM]<sup>+</sup>[BF<sub>4</sub>]<sup>-</sup>), and the surfactant vinyl-SiO<sub>2</sub>. The fabricated materials feature an elastic matrix with microionogel particles embedded in it. The system is chemically and physically cross-linked via vinyl-SiO<sub>2</sub> and Cu<sup>2+</sup>-imidazole coordination interaction, respectively. Such a rational design endows the resulting elastomers with a wide range of properties, including good conductivity, high stretchability, excellent mechanical properties, and self-healability. Besides, owing to this unique structure, they display high stability and their weight and electrical aspects remain almost unchanged in open air and a wide temperature range (30, 50, and 100 °C). Utilizing as flexible sensors, the as-prepared elastomers are able to accurately monitor real-time human motions via converting external stimuli into stable and repeatable signal variations during deformations.



## 1. INTRODUCTION

Ionic liquids (ILs), a kind of molten salt, possess many unique properties, such as high ionic conductivity, chemical and thermal stability, a wide operating window, and low vapor pressure.<sup>1,2</sup> Because of these interesting features, IL-based conductive elastomers (ICEs) consisting of soft elastomeric polymer networks filled with ILs have recently been proposed to construct flexible electronic sensors.<sup>3–5</sup> The fabricated sensors have achieved high sensitivity to a broad range of strains and pressures.<sup>6–8</sup> However, because of the plasticizer effect of ILs, most existing ICEs exhibit low mechanical properties and toughness, and they are prone to damage and fatigue at small strains during the repeated deformation processes.<sup>9,10</sup> Moreover, the as-reported IL-based elastomers suffer from the issues of IL leakage during the practical applications, which thus would cause gradual deterioration in the conductivity of the electronic devices and even potentially affect human health.<sup>11–13</sup> Furthermore, many reported ionogels are unstable under ambient environments because highly hydrophilic ILs can absorb moisture from the air to change their weight, which causes an alternation of various properties including stretchability and conductivity.<sup>14</sup> Thus, it

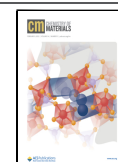
still is a challenging task to develop high-performance IL-based conductors with good mechanical properties and high stability.

In recent years, inspired by natural tissues such as human skin and muscle, soft materials possessing the self-healing capability have emerged and attracted extensive research attention for their promising applications in a myriad of fields.<sup>15–18</sup> Self-healing materials have the ability to repeatedly repair mechanical damage and restore their functionality, thereby significantly improving the durability of the materials and prolonging their service life.<sup>19–21</sup> As for the ICEs, they might suffer from the damage caused by sharp materials or accidental overload because of their high deformability.<sup>22–24</sup> Thus, it is desirable for the ICEs to have beneficial self-healing ability. Although some ICEs have been reported, few of them are intrinsically self-healable.<sup>6,25</sup> Moreover, there is a trade-off

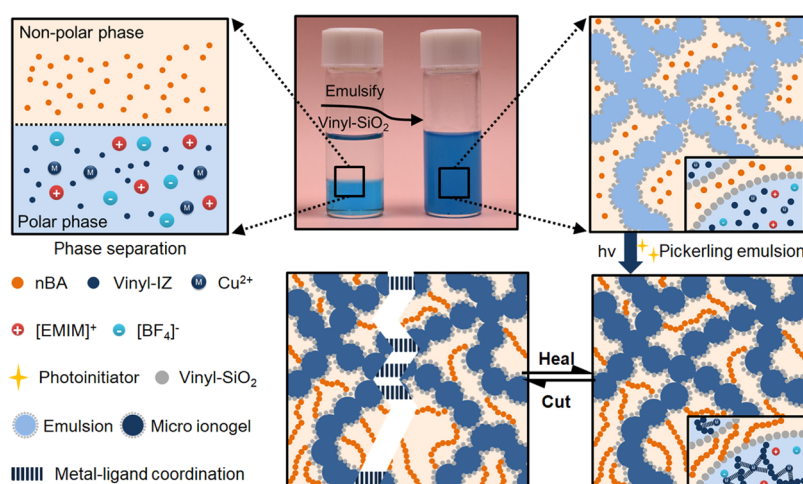
Received: October 12, 2021

Revised: January 5, 2022

Published: January 19, 2022



### Scheme 1. Schematic Illustration of the Microionogel (MIG)-Enhanced Self-Healing Conductive Elastomers via the One-Pot Oil-in-Oil Pickering Emulsion Polymerization



between the self-healing capability and mechanical properties for one material and the enhancement of the mechanical properties usually results in reduced self-healing efficiency.<sup>26–28</sup> To date, the ICEs that have high mechanical strength along with excellent self-healing ability especially under mild conditions have rarely been fabricated.

Herein, we designed and fabricated a high-performance ion-conductive elastomer with integrated high stretchability, good stability, and self-healability via one-pot oil-in-oil Pickering emulsion polymerization (Scheme 1). The obtained ICEs feature an elastic PnBA framework with the integration of MIG particles in which the polyimidazole is dynamically cross-linked through metal–ligand interaction between  $\text{Cu}^{2+}$  and imidazole and ILs are locked into the network. The elastic PnBA phase contributes the large stretchability of the resulting materials. The MIGs act as the cross-linker and conductive filler simultaneously, which endow the obtained elastomers with high mechanical strength, good conductivity, and a wide operating temperature range. Importantly, the ion-conductive elastomers featuring MIGs exhibit excellent stability relative to the conventional ionogels and can self-heal autonomously because of the  $\text{Cu}^{2+}$ -imidazole complexes residing in the MIGs. Using the fabricated ICE, a high-performance strain sensor was constructed, which exhibited high detection sensitivity, rapid response speed, and good antifatigue performance and could monitor different human motions. Therefore, it is expected that the as-prepared IL-based elastomer would be an ideal sensor for a variety of applications of flexible electronic devices.

## 2. EXPERIMENTAL METHODS

**2.1. Materials.** Vinylimidazole (VI) and *n*-butyl acrylate (*n*-BA) and copper acetate ( $\text{Cu}(\text{Ac})_2$ ) were obtained from Sigma-Aldrich Co. The IL (1-butyl-3-methylimidazolium tetrafluoroborate,  $[\text{EMIM}]^+[\text{BF}_4]^-$ ) was purchased from TCI Co. Nanosilica white powders (average diameter was 30 nm), 3-aminopropyl trimethoxysilane, triethylamine,  $\epsilon$ -caprolactone, 2,2-diethoxyacetophenone (DEAP, photoinitiator), and methacryloyl chloride were purchased from Shanghai Aladdin Co. Toluene, tetrahydrofuran, and triethylamine were obtained from Macklin Co. All the solvents were dried through a solvent purification system. The VHB tape was purchased from Minnesota Mining and Manufacturing (3M) Co.

**2.2. Characterization.** Microscope photography was carried out on an Olympus BX-53M instrument, and photographs were analyzed using Image J. Fourier transform infrared (FT-IR) spectra were

obtained using a Nicolet 670 spectrometer with the attenuated total reflectance accessory. Thermal gravimetric analysis (TGA) was performed on a TG 209 F1 from room temperature to 600 °C in an  $\text{N}_2$  atmosphere with a heating rate of 10 °C  $\text{min}^{-1}$ .  $^1\text{H}$  nuclear magnetic resonance ( $^1\text{H}$  NMR) spectra were recorded using an AVANCE III 600 MHz NMR spectrometer at room temperature and  $\text{CDCl}_3$  as the solvent. X-ray photoelectron spectroscopy (XPS) spectra were recorded using a ThermoFisher Scientific Escalab 250X. The conductivity of the ionic conductive elastomer was measured through the four-point probe resistivity test by the 4-Point probe resistivity measurement system (RTS-8) with a size of  $1 \times 5 \times 5 \text{ mm}^3$ .

**2.3. Preparation of the Vinyl- $\text{SiO}_2$ .** The synthesis of the vinyl- $\text{SiO}_2$  was carried out following the method we had reported before.<sup>18,29</sup> At first, 3.5 g silica particles and 5 mL 3-aminopropyl trimethoxysilane were added into a 250 mL flask followed by the addition of toluene (200 mL) to form a uniform solution. After the constant stirring of 12 h at 90 °C, the amino group-modified silica ( $\text{SiO}_2\text{-NH}_2$ ) could be obtained. Next, 1.2 g  $\text{SiO}_2\text{-NH}_2$  and 7.5 g  $\epsilon$ -caprolactone were dissolved in 200 mL tetrahydrofuran. The hydroxyl hybrid silica ( $\text{SiO}_2\text{-R-OH}$ ) could be obtained after the stirring for 12 h at room temperature. Finally, 1.3 g  $\text{SiO}_2\text{-R-OH}$ , 0.5 mL methacryloyl chloride, and 0.45 mL triethylamine were added into 100 mL tetrahydrofuran under vigorous stirring for 12 h at room temperature, and the vinyl- $\text{SiO}_2$  was obtained. All the modified silica particles were collected by centrifugation and stored at 2–8 °C in a nitrogen atmosphere.

**2.4. Preparation of the Stretchable, Stable, and Self-Healable Elastomers via Pickering Emulsion Polymerization.** Using the as-prepared vinyl- $\text{SiO}_2$  nanoparticles as the surfactant, a series of samples with a variable content of MIGs were synthesized, and they are denoted as ICE-MIG- $\chi\%$ , where  $\chi\%$  represents the content of MIG. In a typical procedure, 0.65 mL *n*-BA, 0.25 mL VI, 0.1 mL  $[\text{EMIM}]^+[\text{BF}_4]^-$ , 10 mg 2,2-diethoxyacetophenone, and 2 mg  $\text{Cu}(\text{Ac})_2$  were first mixed under violent stirring. With the introduction of the vinyl- $\text{SiO}_2$  (15 mg/mL), a homogeneous solution could be obtained. The precursor solution was transferred into a PTFE mold ( $30 \times 10 \times 1 \text{ mm}^3$ ) and polymerized under UV light for 1 h ( $\lambda = 365 \text{ nm}$ , power = 8 W), and then the elastomer was obtained. The control samples were fabricated in the same way, except without the introduction of  $\text{Cu}(\text{Ac})_2$ .

## 3. RESULTS AND DISCUSSION

The fabrication process and self-healing mechanism of the IL-based elastomers featuring MIG particles as a conductive filler, PnBA/ $\text{SiO}_2$ /PVI (ILs,  $\text{Cu}^{2+}$ ), are described in Scheme 1. First, the Pickering emulsion stabilized with inorganic nanoparticles was prepared via mixing *n*-BA, VI, ILs,  $\text{Cu}(\text{Ac})_2$ , DEAP, and

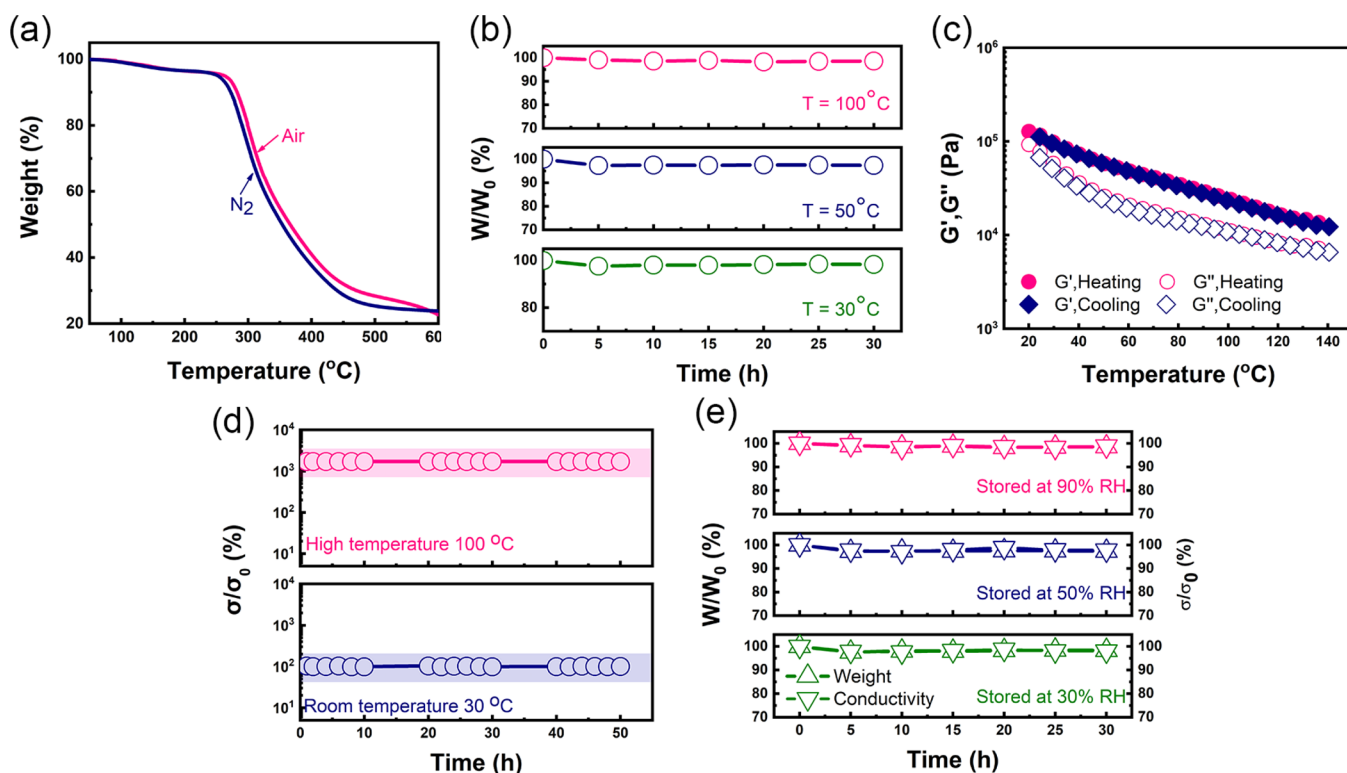


**Figure 1.** (a) Thermogravimetric curve of ICE-MIG; (b) weight stability of the conductive elastomer at different test temperatures; (c) temperature sweeping rheology test for ICE-MIG; (d) stability of the conductivity in the room or extremely high temperature after storing for a long time; (e) weight and conductivity change of ICE-MIG under different humidity in different storage times.

vinyl-SiO<sub>2</sub> together. Upon ultraviolet light irradiation, the polymeric network was formed to offer the IL-based elastomers, which is chemically cross-linked via vinyl-SiO<sub>2</sub> as a cross-linker and physically cross-linked via dynamic Cu<sup>2+</sup>-imidazole coordination interaction. The chemical bonds would attribute to enhancement of the material's mechanical properties, while the dynamically physical bonds endow the obtained materials with excellent self-healing ability. Most importantly, considering the delicate designed architecture, it is envisioned that instability in open air and IL leakage during repeated deformation could be well solved.

The vinyl-SiO<sub>2</sub> nanoparticles, which play the dual roles of a surfactant and cross-linker, were prepared according to the procedure illustrated in Scheme S1. The long hydrophobic alkyl chain was elaborately introduced between the end vinyl group and the surface of SiO<sub>2</sub>, which showed an obvious effect on enhancing the stability of the Pickering emulsion.<sup>30</sup> The successful preparation of the vinyl-SiO<sub>2</sub> was confirmed by FT-IR and TGA techniques. As shown in Figure S1b, the peaks at 3130–3700 cm<sup>-1</sup> and 1720 cm<sup>-1</sup> could be attributed to the surface -OH and C=O group stretching vibration, respectively, implying the successful introduction of the aliphatic hydroxylated chain onto the surface of silica. In Figure S1c, the peaks observed at 1670 and 940 cm<sup>-1</sup> originated from the characteristic stretching of the vinyl groups.<sup>31,32</sup> Meanwhile, in comparison with SiO<sub>2</sub>-NH<sub>2</sub>, SiO<sub>2</sub>-R-OH and vinyl-SiO<sub>2</sub> exhibited increasing weight loss (8 and 36%), further informing the successful tethering of aliphatic vinyl chains onto the surface of silica (Figure S2).<sup>32</sup> In addition, the sharp weight loss at ~180 °C of vinyl-SiO<sub>2</sub> could be ascribed to the instability of vinyl functional groups at high temperatures.

Using the as-prepared vinyl-SiO<sub>2</sub> as a surfactant, the oil-in-oil Pickering emulsion was prepared by mixing active monomers, photoinitiator, ILs, and copper salt under violent stirring. The effect of vinyl-SiO<sub>2</sub> on the stability of the formed Pickering emulsion can be obviously observed from Scheme 1. Owing to the big polarity difference, the solution displayed layered phase separation without vinyl-SiO<sub>2</sub>, while the color difference completely disappeared in the presence of vinyl-SiO<sub>2</sub>, implying the formation of a stable Pickering emulsion. The prepared Pickering emulsions stabilized with vinyl-SiO<sub>2</sub> were further observed by confocal fluorescence microscopy. The polarized micrographs took the characteristic structure of Pickering emulsion, as shown in Figure S3. The determined size of the droplets analyzed using Image J was in the range of 5–20 μm (Figure S4).

Being irradiated by ultraviolet light, the as-prepared Pickering emulsion polymerized to produce the targeting ICEs PnBA/SiO<sub>2</sub>/PVI-ILs. The <sup>1</sup>H NMR spectrum of the as-prepared elastomer shows that the characteristic signals belonging to the vinyl monomers (*n*-BA and VI) were not observed, confirming that there was no unreacted monomer in the material (Figure S5). The *n*-BA phase formed the elastic matrix, while the droplets containing VI monomers, ILs, and copper salt formed the MIG particles as conductive fillers. As the MIG particles were embedded into the hydrophobic PnBA matrix, IL leakage and moisture absorption can be prevented, so the obtained materials should possess excellent air and conductive stability. As shown in the thermogravimetric curve (Figure 1a), the elastomers exhibited ultrahigh temperature tolerance (the decomposition temperature up to 225 °C in air and 230 °C in N<sub>2</sub>, respectively), which was much higher than that of the conventional gel-based electrolytes. Meanwhile,

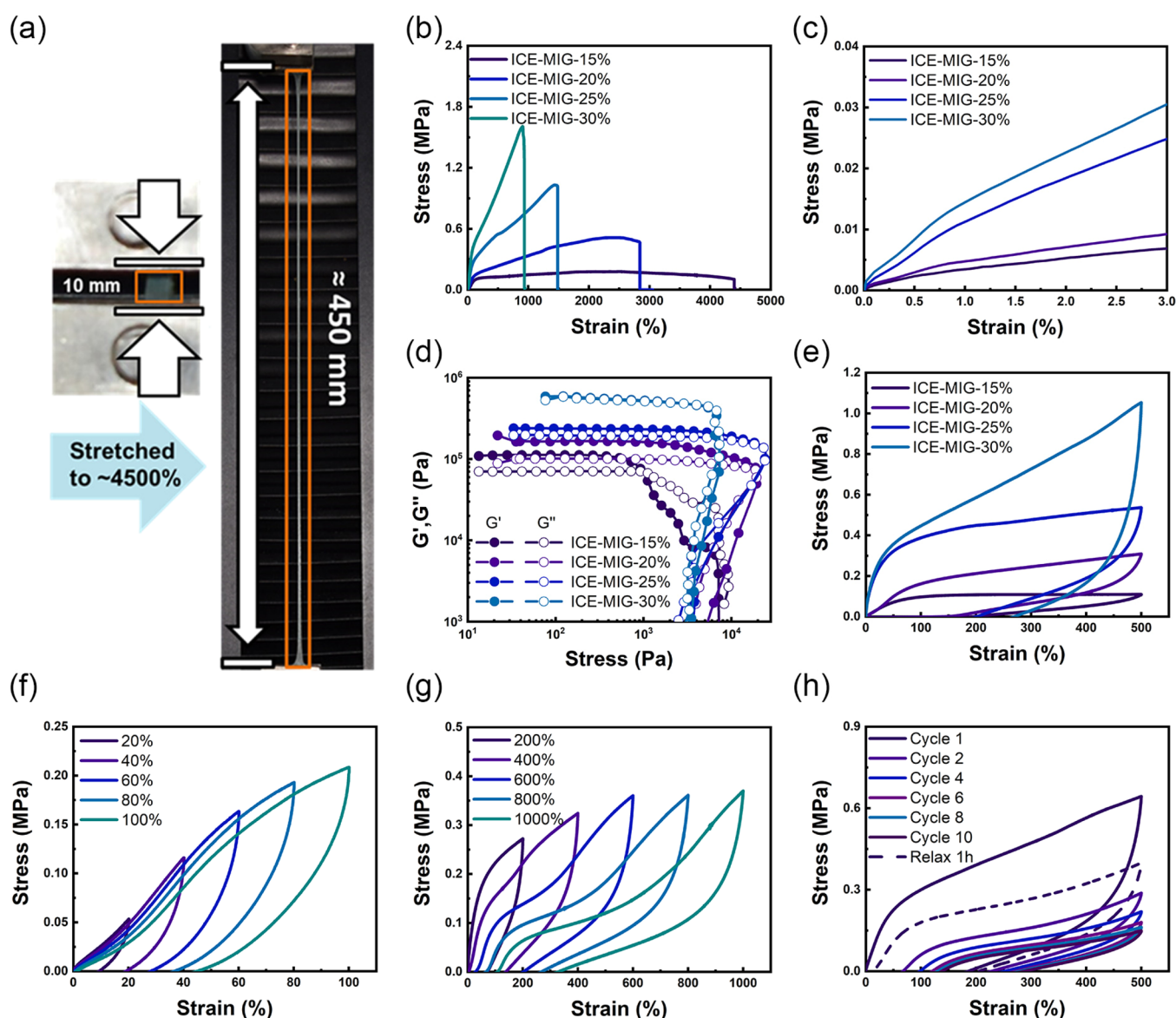


**Figure 2.** (a) Digital photograph of ICE-MIG-15% before and upon stretching; (b) stress–strain curves of the elastomers with different concentrations of the MIGs; (c) tensile curves of the elastomers in the small strain range; (d) rheological stress sweeping measurements of different samples with a shear frequency of 5 rad/s; (e) loading–unloading test of the different samples at a maximum strain of 500%; successive stretching–releasing tests upon ICE-MIG-25% (f) in the small strain range (20–100%), and (g) in the large strain range (200–1000%) without resting time in each cycle; (h) repeated cyclic stress–strain curves of ICE-MIG-25% at a maximum strain of 500%.

they showed excellent stability in a broad range of temperatures under ambient conditions, and their weight remained almost unchanged even after being stored for 30 h at 100 °C (Figure 1b). Temperature sweep measurement was further performed to investigate the material's stability (Figure 1c). During the whole temperature range (20–140 °C), the conductive elastomer retained the solid-like state as the storage modulus ( $G'$ ) was always higher than the loss modulus ( $G''$ ). Notably, the modulus–temperature curves were almost overlapping in two stages (heating and cooling), demonstrating that the elastomers had cycling thermal stability. The elastomers also displayed stable conductivity, which was confirmed by the material's relative conductivity ( $\sigma/\sigma_0$ ) remaining nearly constant at low temperature (30 °C) or high temperature (100 °C) for more than 50 h (Figure 1d). The excellent thermal stability of the fabricated ionic elastomers ICE-MIG should be attributed to the unique

features of ILs and their unique structure featuring MIG particles being embedded into the PnBA matrix, which could efficiently prevent the evaporation and leakage of ILs. The effect of humid conditions on the properties of the prepared conductive elastomer was further investigated, as shown in Figure 1e. After the long-term storage (more than 30 h) under different humidity conditions, the weight and conductivity of the elastomers remained almost unchanged, indicating the excellent humidity insensitivity and stability. These results indicated that the fabricated elastomers could be used in a wide range of temperatures in open air because of the combination of high thermal and air stability.

The as-prepared elastomers are chemically and physically cross-linked via the vinyl-SiO<sub>2</sub> located on the interface of the PnBA matrix and ionogels and the dynamic Cu<sup>2+</sup>-imidazole coordination interaction inside the ionogels. The synergistic effect of chemical bonds and metal–ligand coordination would

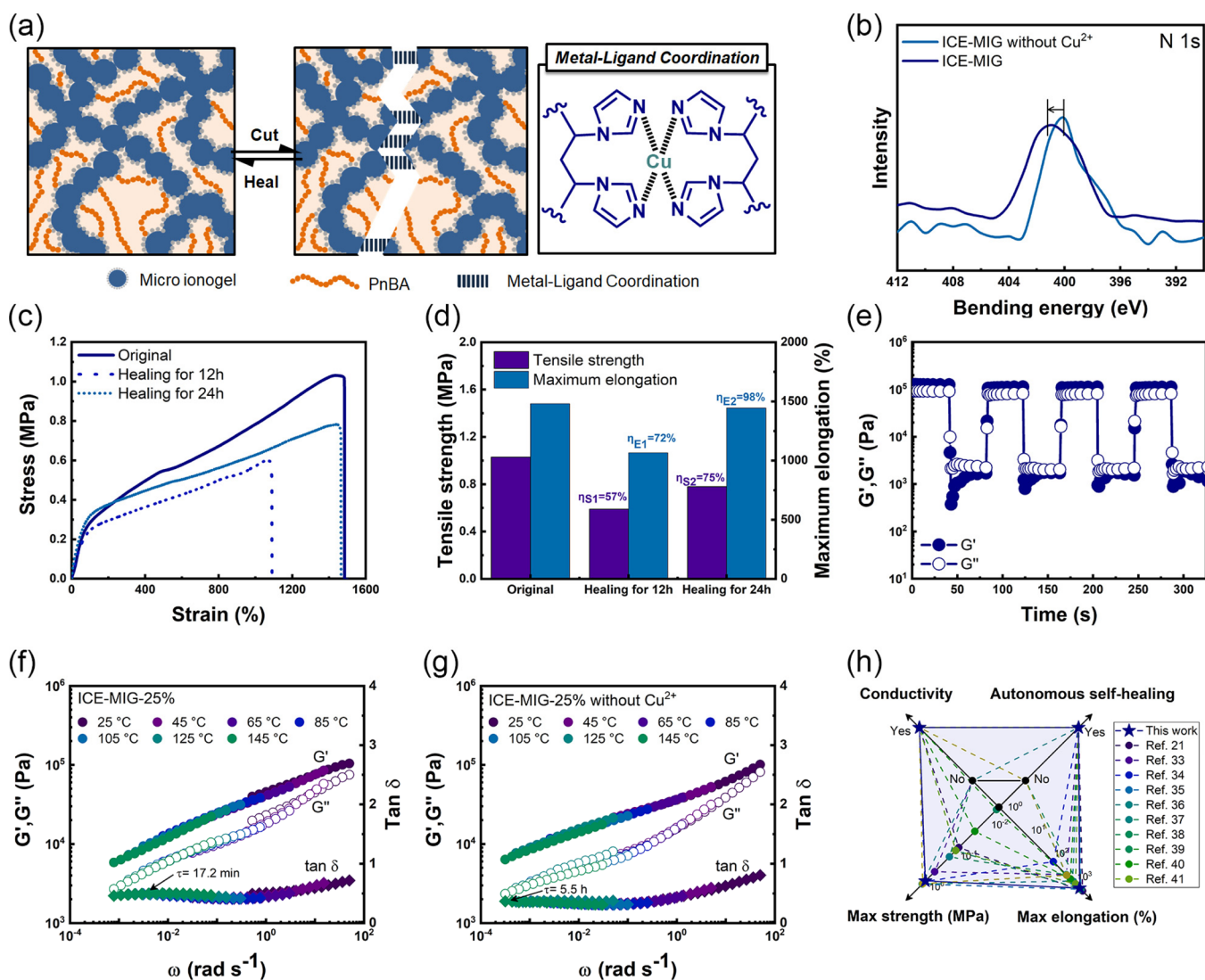


**Figure 3.** (a) Schematic illustration of the self-healing performance of ICE-MIG-25%; (b) XPS spectra of the N 1s region of ICE-MIG-25% and the control sample without Cu<sup>2+</sup>; (c) tensile curves of ICE-MIG-25% in the original and healed (healing for 12 and 24 h in the standard atmosphere, 25 °C, RH = 50%) state; (d) summary of the tensile strength and maximum elongation of the conductors in different states; (e) dynamic sweeping rheology test of the conductor; dynamic mechanical behaviors of (f) ICE-MIG-25% and (g) ICE-MIG-25% without Cu<sup>2+</sup>; (h) comparison between ICE-MIG-25% and the other conductors reported previously.

endow the obtained elastomers with improved mechanical properties. Figure 2a shows that the prepared conductive elastomer possessed a high stretchability. In particular, ICE-MIG-15% could be stretched to almost 45 times its original length, which was better than that of ordinary conductive elastomers. A series of tests had been conducted to investigate the mechanical properties of the elastomers. The tensile curves of the elastomers with different ionogel contents are shown in Figure 2b. In particular, the sample ICE-MIG-15% exhibited an ultrastretchability with 4450% maximum elongation at break. Meanwhile, it is observed that the tensile properties of the as-prepared elastomers were obviously enhanced with the increase of the MIG contents. The fracture stress of the elastomers increased from 150 kPa to 1.61 MPa with the increase in the content of the MIGs from 15 to 30%. Furthermore, with the increase of the content of MIG particles, Young's modulus of the as-prepared elastomers gradually increased from 0.20 to 0.94 MPa in the small strain range (Figure 2c). In addition, the effect of Cu<sup>2+</sup>-imidazole

coordination on the mechanical properties of the materials is also investigated. The maximum elongation and strength at break of the control sample without Cu<sup>2+</sup> (1190% and 0.47 MPa) are much lower than those (1460% and 1.03 MPa) of the sample with Cu<sup>2+</sup> (Figure S6). The elastomer ICE-MIG-25% reached superior mechanical properties with a fracture strength of 1.03 MPa and a fracture strain of 1460%; thus it was used as the optimal sample for the following measurements unless otherwise mentioned.

Because of the synergistic effect of dense chemical bonds and dynamic Cu<sup>2+</sup>-imidazole coordination interaction, the resulting polymeric network should have excellent mechanical properties. The rheological sweeping test was performed to investigate the samples, and all the samples exhibited a solid-like state ( $G' > G''$ ) in the low-stress range, which further confirms the cross-linking presence in the system (Figure 2d). Subsequently, a series of cyclic tensile loading–unloading tests were performed. First, the cyclic tensile test was conducted on the elastomers with different contents of the MIGs at a

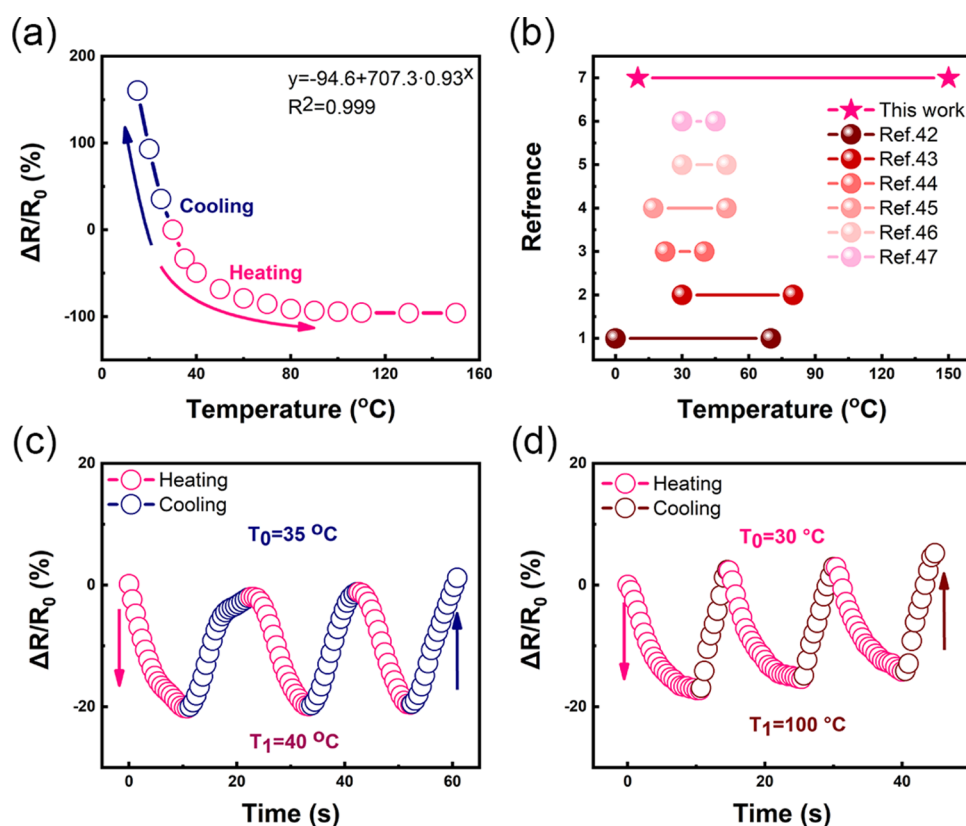


**Figure 4.** (a) Resistance–temperature relative curve of the ICE-based thermoresistive sensor in a wide temperature range (10–150 °C); (b) comparison of the detection temperature range between this work and the previous work; the uninterrupted step temperature sweeping test at (c) room temperature (35–40 °C) and (d) extremely high temperature (90–100 °C).

maximum strain of 500%, which exceeds the strain range of most normal carbon material composite elastomers (Figure 2e). An obvious hysteresis loop was observed for each sample, and the hysteresis loop area increased with the increase of the MIG content, implying efficient energy dissipation via the fracture and reconstruction of  $\text{Cu}^{2+}$ -imidazole coordination. Using the elastomer ICE-MIG-25% as the optimal sample, the cyclic tensile tests with different strain were further performed to evaluate the toughness and elastic properties of the elastomers. First, cyclic tensile tests were performed within a small strain range (20–100%) without waiting time between two consecutive loadings. Figure 2f shows that the elastomer could almost recover its original state in every cycle, revealing that the elastomer possessed excellent resilience within the strain of 100% feasible for many practical applications. Second, cyclic tensile tests were performed within a large strain range (200–1000%) (Figure 2g). Larger hysteresis loops were observed with the maximum strain increasing from 200 to 1000%, because of the break of more covalent bonds during deformations. To further demonstrate the cycling stability of the prepared elastomer, 10 repeated cyclic tensile tests without waiting time between two consecutive tests were performed under a larger strain of 500%. As shown in Figure 2h, the curve in the first cycle displayed a pronounced hysteresis loop, which indicated a significant energy dissipation through the rupture of the dynamic bonds during the stretching process. As compared, the hysteresis loop in the first cycle was much larger than others because the broken dynamic bonds could not rapidly recover to their original state. In sequential tests, the hysteresis loop slightly decreased with the increase of the cycle because of the reformation of the dynamic bonds. It is worth

mentioning that, after resting for 1 h at room temperature, the fracture stress of the sample recovered to almost 50% that of the first cycle, implying the good elastic recoverability of the prepared elastomers.

Benefiting from the concentrated dynamic metal–ligand coordination bonds in the MIGs, ICE-MIG-25% exhibited self-healing performance at room temperature (Figure 3a). As shown in Figure 3b, ICE-MIG-25% showed a higher intensity of N 1s compared with the control sample without  $\text{Cu}^{2+}$ , indicating the successful formation of the  $\text{Cu}^{2+}$ -imidazole coordination complexes. The binding energy of  $\text{Cu}^{2+}$ -imidazole was about 401 eV. The tensile tests in different healing times were conducted to investigate the healing efficiency of the conductive elastomer (Figure 3c). After healing for 12 h, the tensile strength and maximum elongation could recover to 0.59 MPa and 1067%, respectively. By further extending the healing time to 24 h, the elongation ratio at break recover almost completely and the healing ratio was up to 98% (Figure 3d). By contrast, the control sample (ICE-MIG-25% without  $\text{Cu}^{2+}$ ) did not exhibit self-healing performance (Figure S7). Then, the dynamic sweeping rheology test was conducted to investigate the self-healing behavior of ICE-MIG-25%. As shown in Figure 3e, the storage modulus ( $G'$ ) was higher than the loss modulus ( $G''$ ) as the shear strain was 0.5%, indicating that the elastomer remained in the solid-like state. However,  $G''$  surpassed  $G'$  as the shear strain shifted from 0.5 to 100%, indicating the rupture of the polymer network. Once the strain shifted back to 0.5%,  $G'$  and  $G''$  recovered instantly and completely, confirming the immediate self-healability of the prepared elastomers. Rheological master curves at a reference temperature of 25 °C showed that the resultant elastomer displayed

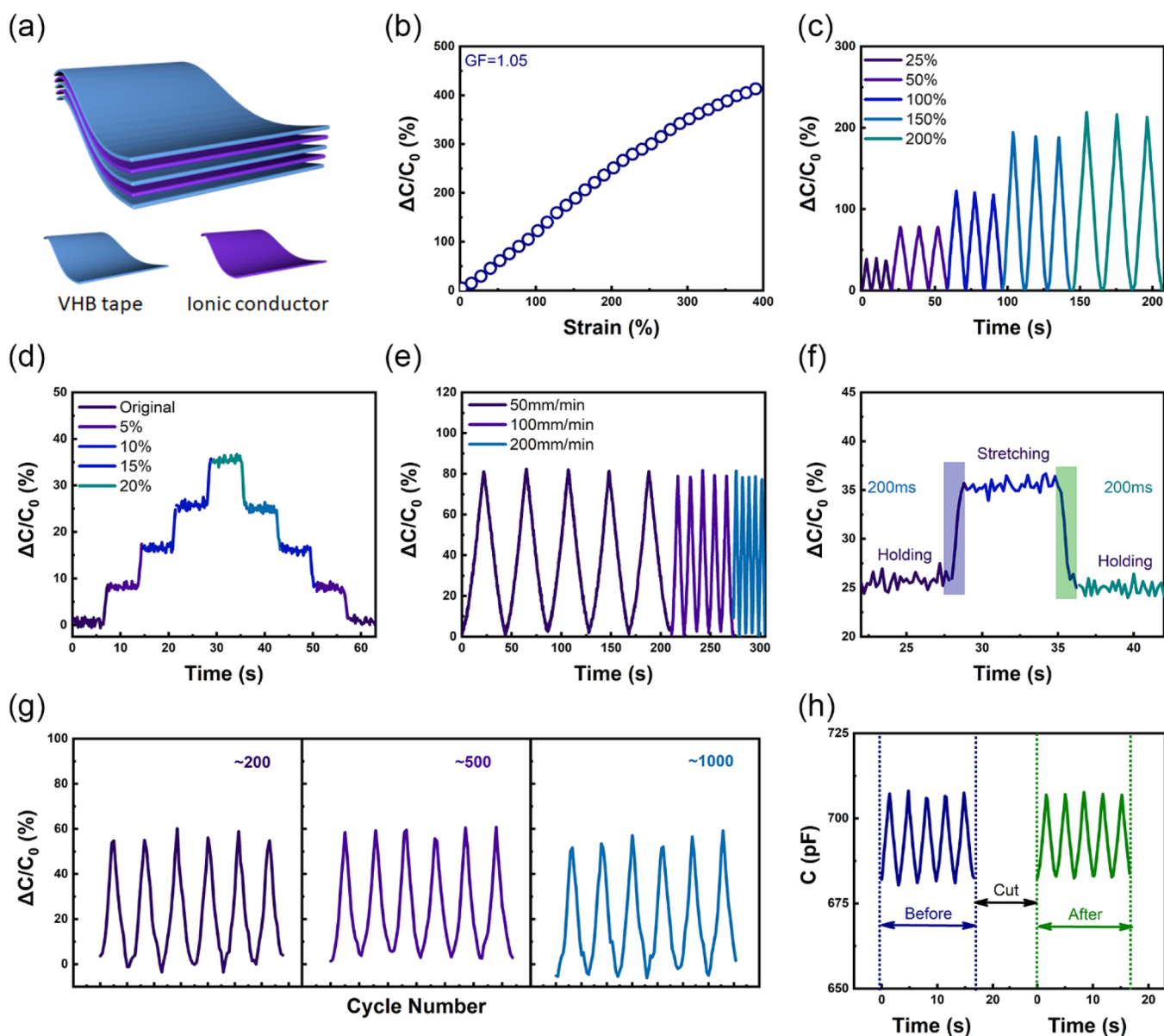


**Figure 5.** (a) Schematic illustration of the ICE-based capacitance sensor; (b) capacitance relative curve of the sensor in the range of 0–400%; (c) capacitance patterns at different strains; (d) electronic signals in the stepwise stretching–releasing tests in the small strain range (5–25%); (e) capacitance–strain curves at increased stretching rates (50–200 mm/min); (f) sensing response time of the sensor; (g) cyclic test of the electronic sensor for 1000 cycles at a strain of 50%; (h) comparison of electronic patterns of the sensor before and after self-healing.

elastic state ( $G' > G''$ ) over the whole frequency range and its dynamic modulus followed time–temperature superposition (Figure 3f,g). The relaxation time was estimated according to the viscoelastic peak in the master curve. The relaxation time for the sample with  $\text{Cu}^{2+}$  (17.2 min) was much shorter than that of the sample without  $\text{Cu}^{2+}$  (5.5 h). The short relaxation time indicates the rapid self-healing kinetics. Compared with the currently reported stretchable conductors, this elastomer system possessed the combination of excellent modulus, high stretchability, autonomous self-healing, intrinsic conductivity, and stability in a wide range of temperatures under open air.<sup>21,33–41</sup> As we know, there is a trade-off between the material's modulus, self-healing efficiency, and stretchable ratio, and the improvement of the material's modulus commonly leads to reduced self-healing efficiency and elongation ratio. Thus, the conductive elastomers, which maintain a high modulus as well as good stretchability and

autonomous self-healing, have been rarely reported in the literature, as displayed in Figure 3h.

Based on the temperature responsiveness and stability, the as-prepared elastomers could be assembled into a simple resistive thermosensitive sensor to monitor the outside thermal stimulus (Figure S8). Resulting from the different migration rates of the ions at different temperatures, the sensor's resistance exhibited a temperature-dependent behavior, and it could be approximately fitted to an exponential function ( $y = -94.6 + 707.3 \times 0.93^x$ ), with a high coefficient of determination ( $R^2 = 0.999$ ) (Figure 4a). Notably, because of the advantages of the low saturated vapor and high thermal stability of ILs, the IL-based thermosensitive sensor exhibited an extremely wide temperature application range (10–150 °C), which was significantly wider than that of most of the reported thermosensitive sensors (Figure 4b).<sup>42–47</sup> The uninterrupted step temperature sweeping test was conducted

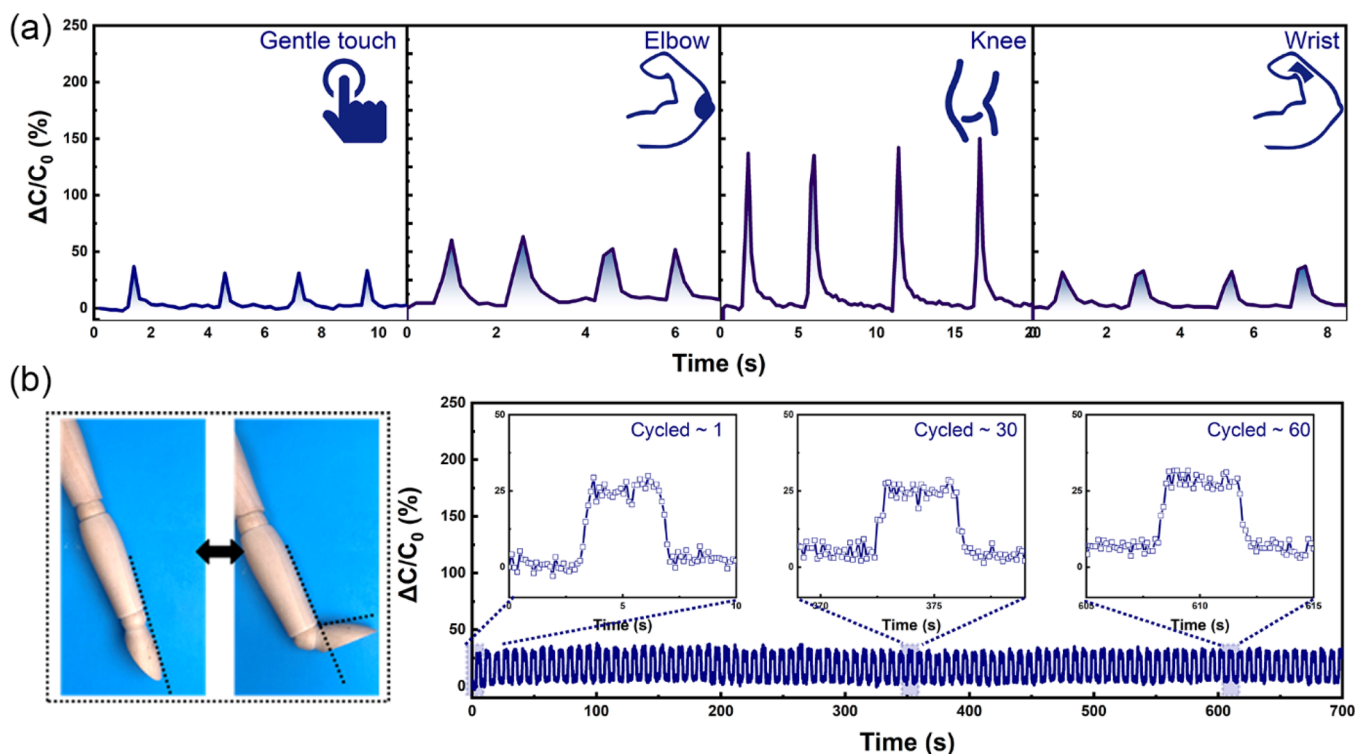


**Figure 6.** ICE-based sensor was attached on a puppet, simulating the movement of the human body, to monitor the human motion. (a) Electronic patterns of the puppet was gentle touching, bending the elbow, bending the knee, and bending the wrist, respectively. (b) 70 subsequent capacitance responses at a wrist bending angle of 80°.

to assess the thermal sensitivity (Figure 4c,d). With the precise temperature control of the heating source, the resistance curve displayed a wavy shape in the range of the near-body surface temperature (35–40 °C). Additionally, in the high temperature range (90–100 °C), the sensor could also respond sensitively to the change of the temperature.

The MIG composite conductive elastomer could be fabricated into the capacitive mode strain sensor with the multilayer structure for the future human motion monitoring. Typically, a capacitance sensor was fabricated by integrating two pieces of ICE-MIG-25% with a VHB tape and then sealed by two pieces of VHB tape again (Figure 5a). The relationship between the deformation of the device and the capacitance follows eq 1:

$$C = \frac{\epsilon s}{4\pi kd} \quad (1)$$

where  $C$  is the capacitance,  $\epsilon$  represents the dielectric constant of the middlemost VHB tape (serving as the dielectric layer),  $k$  is the electrostatic constant,  $s$  is on behalf of the effective area of the elastomer (serving as the conducting layer), and  $d$  is the thickness of the dielectric layer. Upon the sensor being stretched, the expanding area of the elastomer would result in the increase of the capacitance, which could be recorded by the LCR meter. Figure 5b shows the relative capacitance changes versus the applied strain ranging from 0 to 400%. The relative curve was nearly linear with a GF of 1.05, indicating the high detection sensitivity of the sensor. Applied with the increasing strain (25–200%) at a fixed strain speed, the relative resistant changes gradually increased, and the electric signals were stable and repeatable during the stretching, further demonstrating the sensor's high conductive stability (Figure 5c). In addition, this strain sensor showed excellent detection accuracy, and the

deformation with small strains (<25%) could also be detected sensitively. As demonstrated in Figure 5d, the relative capacitance changes increased stepwise with the strain increasing from 5 to 25% during the stretching process. While in the sensor-releasing process, the capacitance response returned to the original value. It should be noted that the capacitance change during the releasing process remained the same height as that in the stretching process. In Figure 5e, the capacitance change level of the sensor remained relatively steady under 50% strain when the deformation rate increased from 50 to 200 mm/min, implying its excellent frequency tolerance. In addition, the sensor exhibited fast response and recovery times of 200 ms, which are comparable to those reported in the literature (Figure 5f). In the cycling tests, this sensor still exhibited excellent cycling stability without an obvious shift of the baseline in the whole procession during 1000 cycles (Figure 5g). Finally, benefiting from the self-healing performance of ICE-MIG-25%, the ICE-based sensor also exhibited an excellent self-repairable sensing property. As shown in Figure 5h, the capacitive pattern of the healed sensor was similar to the original state after healing for 12 h.

To further investigate the practical application performance, the ICE-based sensor was attached to the puppet to monitor the real-time activities. Figure 6a shows that the electronic signals correspondingly changed as we gently touched the puppet and bent its elbow, knee, and wrist, respectively. Notably, all the signal patterns were repeatable and the baseline was always stable. To evaluate the circulation stability of the ICE-based sensor for practical applications, 70 subsequent tests at a wrist bending angle of 80° were conducted (Figure 6b). During the whole process, this sensor exhibited stable sensing performance without any obvious

response deviation, attributing to the excellent flexibility and remarkable durability.

#### 4. CONCLUSIONS

In summary, this investigation reported a new class of ICEs featuring MIG particles as conductive fillers via facile one-pot Pickering emulsion polymerization. The resulting materials exhibited unique properties which contributed to ILs, including good conductivity and a wide operating temperature range. In addition, the elastomers are highly stretchable, mechanically robust, and sensitive to a board range of strains. Moreover, owing to the  $\text{Cu}_2^+$ -imidazole interaction inside PVI-ILs, the elastomers displayed the advantage of a spontaneous self-healing property at room temperature without needing any external stimuli, which is crucial for prolonging the service life of the flexible electronic devices. Importantly, the as-prepared elastomers exhibited high stability without the issues of weight change and IL leakage confronted by conventional IL-based elastomers. Considering these desirable functionalities, the as-prepared elastomers were employed to assemble into strain sensors, which could accurately detect various human motions. Overall, a new simple yet efficient strategy was developed for the fabrication of stable IL-based elastomers, which can further be extended to fabricate new types of IL-based elastomers because of the diversity of the elastic matrix and ILs.

#### ■ ASSOCIATED CONTENT

##### SI Supporting Information

The Supporting Information is available free of charge at <https://pubs.acs.org/doi/10.1021/acs.chemmater.1c03547>.

Mechanical measurements, sensing performance and human detection. Scheme S1: Synthesis of surface-modified vinyl-SiO<sub>2</sub>. Figures S1–S8: FT-IR spectra, TGA curve of the modified silica; confocal fluorescence microscopy morphologies, and the corresponding diameter distribution of the emulsion; <sup>1</sup>H NMR spectra of ICE-MIG; tensile stress–strain curves of ICE-MIG-25% and the control sample; the tensile curves of the control sample in the original and healed state; and schematic illustration of the thermoresistive sensor (PDF)

#### ■ AUTHOR INFORMATION

##### Corresponding Authors

**Xiaoshan Fan** – State Key Laboratory for Modification of Chemical Fibers and Polymer Materials, College of Materials Science and Engineering, Innovation Center for Textile Science and Technology, Donghua University, Shanghai 201620, P. R. China; [orcid.org/0000-0002-0617-7400](https://orcid.org/0000-0002-0617-7400); Email: [xsfan@dhu.edu.cn](mailto:xsfan@dhu.edu.cn)

**Tianxi Liu** – State Key Laboratory for Modification of Chemical Fibers and Polymer Materials, College of Materials Science and Engineering, Innovation Center for Textile Science and Technology, Donghua University, Shanghai 201620, P. R. China; Key Laboratory of Synthetic and Biological Colloids, Ministry of Education, School of Chemical and Material Engineering, Jiangnan University, Wuxi 214122, P. R. China; [orcid.org/0000-0002-5592-7386](https://orcid.org/0000-0002-5592-7386); Email: [txliu@fudan.edu.cn](mailto:txliu@fudan.edu.cn)

#### Authors

**Xiaohui Yu** – State Key Laboratory for Modification of Chemical Fibers and Polymer Materials, College of Materials Science and Engineering, Innovation Center for Textile Science and Technology, Donghua University, Shanghai 201620, P. R. China

**Yong Zheng** – State Key Laboratory for Modification of Chemical Fibers and Polymer Materials, College of Materials Science and Engineering, Innovation Center for Textile Science and Technology, Donghua University, Shanghai 201620, P. R. China

**Yufei Wang** – State Key Laboratory for Modification of Chemical Fibers and Polymer Materials, College of Materials Science and Engineering, Innovation Center for Textile Science and Technology, Donghua University, Shanghai 201620, P. R. China

**Haopeng Zhang** – State Key Laboratory for Modification of Chemical Fibers and Polymer Materials, College of Materials Science and Engineering, Innovation Center for Textile Science and Technology, Donghua University, Shanghai 201620, P. R. China

**Hui Song** – State Key Laboratory for Modification of Chemical Fibers and Polymer Materials, College of Materials Science and Engineering, Innovation Center for Textile Science and Technology, Donghua University, Shanghai 201620, P. R. China

**Zibiao Li** – Institute of Materials Research and Engineering, Agency for Science, Technology and Research (A\*STAR), Singapore 138634, Singapore; [orcid.org/0000-0002-0591-5328](https://orcid.org/0000-0002-0591-5328)

Complete contact information is available at: <https://pubs.acs.org/doi/10.1021/acs.chemmater.1c03547>

#### Author Contributions

The manuscript was written through contributions of all authors. All authors have given approval to the final version of the manuscript.

#### Notes

The authors declare no competing financial interest.

#### ■ ACKNOWLEDGMENTS

The authors are grateful for the financial support from the National Natural Science Foundation of China (51773035), the Shanghai Rising-Star Program (18QA1400200), and the Shanghai Scientific and Technological Innovation Project (18JC1410600).

#### ■ REFERENCES

- (1) Amarasekara, A. S. Acidic Ionic Liquids. *Chem. Rev.* **2016**, *116*, 6133–6183.
- (2) Hejazifar, M.; Lanaridi, O.; Bica-Schröder, K. Ionic liquid based microemulsions: A review. *J. Mol. Liq.* **2020**, *303*, No. 112264.
- (3) Jiang, N.; Li, H.; Hu, D.; Xu, Y.; Hu, Y.; Zhu, Y.; Han, X.; Zhao, G.; Chen, J.; Chang, X.; Xi, M.; Yuan, Q. Stretchable strain and temperature sensor based on fibrous polyurethane film saturated with ionic liquid. *Compos. Commun.* **2021**, *27*, No. 100845.
- (4) Park, D. H.; Park, H. W.; Chung, J. W.; Nam, K.; Choi, S.; Chung, Y. S.; Hwang, H.; Kim, B.; Kim, D. H. Highly Stretchable, High-Mobility, Free-Standing All-Organic Transistors Modulated by Solid-State Elastomer Electrolytes. *Adv. Funct. Mater.* **2019**, *29*, No. 1808909.
- (5) Wang, Y.; Sun, S.; Wu, P. Adaptive Ionogel Paint from Room-Temperature Autonomous Polymerization of  $\alpha$ -Thioctic Acid for

Stretchable and Healable Electronics. *Adv. Funct. Mater.* **2021**, *31*, No. 2101494.

(6) Cao, Z.; Liu, H.; Jiang, L. Transparent, mechanically robust, and ultrastable ionogels enabled by hydrogen bonding between elastomers and ionic liquids. *Mater. Horiz.* **2020**, *7*, 912–918.

(7) Lei, Z.; Wu, P. A highly transparent and ultra-stretchable conductor with stable conductivity during large deformation. *Nat. Commun.* **2019**, *10*, 3429.

(8) Li, T.; Wang, Y.; Li, S.; Liu, X.; Sun, J. Mechanically Robust, Elastic, and Healable Ionogels for Highly Sensitive Ultra-Durable Ionic Skins. *Adv. Mater.* **2020**, *32*, No. 2002706.

(9) Peng, N.; Lv, R.; Jin, T.; Na, B.; Liu, H.; Zhou, H. Thermal and strain-induced phase separation in an ionic liquid plasticized polylactide. *Polymer* **2017**, *108*, 442–448.

(10) Wang, J.; Liang, Y.; Zhang, Z.; Ye, C.; Chen, Y.; Wei, P.; Wang, Y.; Xia, Y. Thermoplastic starch plasticized by polymeric ionic liquid. *Eur. Polym. J.* **2021**, *148*, No. 110367.

(11) Cho, C.-W.; Pham, T. P. T.; Zhao, Y.; Stolte, S.; Yun, Y.-S. Review of the toxic effects of ionic liquids. *Sci. Total Environ.* **2021**, *786*, No. 147309.

(12) Gao, N.; He, Y.; Tao, X.; Xu, X.-Q.; Wu, X.; Wang, Y. Crystal-confined freestanding ionic liquids for reconfigurable and repairable electronics. *Nat. Commun.* **2019**, *10*, 547.

(13) Yan, F.; Lan, T.; Yan, X.; Jia, Q.; Wang, Q. Norm index-based QSTR model to predict the eco-toxicity of ionic liquids towards Leukemia rat cell line. *Chemosphere* **2019**, *234*, 116–122.

(14) Okafuji, A.; Kohno, Y.; Nakamura, N.; Ohno, H. Design of thermoresponsive poly(ionic liquid) gels containing proline units to catalyze aldol reaction in water. *Polymer* **2018**, *134*, 20–23.

(15) Tan, Y. J.; Susanto, G. J.; Anwar Ali, H. P.; Tee, B. C. K. Progress and Roadmap for Intelligent Self-Healing Materials in Autonomous Robotics. *Adv. Mater.* **2021**, *33*, No. 2002800.

(16) Khatib, M.; Zohar, O.; Haick, H. Self-Healing Soft Sensors: From Material Design to Implementation. *Adv. Mater.* **2021**, *33*, No. 2004190.

(17) Xu, S.; Li, J.; Qiu, H.; Xue, Y.; Yang, J. Repeated self-healing of composite coatings with core-shell fibres. *Compos. Commun.* **2020**, *19*, 220–225.

(18) Yu, X.; Zheng, Y.; Zhang, H.; Wang, Y.; Fan, X.; Liu, T. Fast-Recoverable, Self-Healable, and Adhesive Nanocomposite Hydrogel Consisting of Hybrid Nanoparticles for Ultrasensitive Strain and Pressure Sensing. *Chem. Mater.* **2021**, *33*, 6146–6157.

(19) Xu, K.; Wang, Y.; Zhang, B.; Zhang, C.; Liu, T. Stretchable and self-healing polyvinyl alcohol/cellulose nanofiber nanocomposite hydrogels for strain sensors with high sensitivity and linearity. *Compos. Commun.* **2021**, *24*, No. 100677.

(20) Mao, J.; Zhao, C.; Li, Y.; Xiang, D.; Wang, Z. Highly stretchable, self-healing, and strain-sensitive based on double-crosslinked nanocomposite hydrogel. *Compos. Commun.* **2020**, *17*, 22–27.

(21) Cao, Y.; Tan, Y. J.; Li, S.; Lee, W. W.; Guo, H.; Cai, Y.; Wang, C.; Tee, B. C. K. Self-healing electronic skins for aquatic environments. *Nat. Electron.* **2019**, *2*, 75–82.

(22) Xie, Y.; Xie, R.; Yang, H.-C.; Chen, Z.; Hou, J.; López-Barrón, C. R.; Wagner, N. J.; Gao, K.-Z. Iono-Elastomer-Based Wearable Strain Sensor with Real-Time Thermomechanical Dual Response. *ACS Appl. Mater. Interfaces* **2018**, *10*, 32435–32443.

(23) Lei, Z.; Wu, P. Adaptable polyionic elastomers with multiple sensations and entropy-driven actuations for prosthetic skins and neuromuscular systems. *Mater. Horiz.* **2019**, *6*, 538–545.

(24) Wang, Y.; Liu, Y.; Plamthottam, R.; Tebyetekerwa, M.; Xu, J.; Zhu, J.; Zhang, C.; Liu, T. Highly Stretchable and Reconfigurable Ionogels with Unprecedented Thermoplasticity and Ultrafast Self-Healability Enabled by Gradient-Responsive Networks. *Macromolecules* **2021**, *54*, 3832–3844.

(25) Sun, L.; Chen, S.; Guo, Y.; Song, J.; Zhang, L.; Xiao, L.; Guan, Q.; You, Z. Ionogel-based, highly stretchable, transparent, durable triboelectric nanogenerators for energy harvesting and motion sensing over a wide temperature range. *Nano Energy* **2019**, *63*, 103847.

(26) Sun, L.; Huang, H.; Ding, Q.; Guo, Y.; Sun, W.; Wu, Z.; Qin, M.; Guan, Q.; You, Z. Highly Transparent, Stretchable, and Self-Healable Ionogel for Multifunctional Sensors, Triboelectric Nanogenerator, and Wearable Fibrous Electronics. *Adv. Fiber Mater.* **2021**, DOI: 10.1007/s42765-021-00086-8.

(27) Zhang, L.; Liu, Z.; Wu, X.; Guan, Q.; Chen, S.; Sun, L.; Guo, Y.; Wang, S.; Song, J.; Jeffries, E. M.; He, C.; Qing, F.-L.; Bao, X.; You, Z. A Highly Efficient Self-Healing Elastomer with Unprecedented Mechanical Properties. *Adv. Mater.* **2019**, *31*, No. 1901402.

(28) Li, Y.; Li, W.; Sun, A.; Jing, M.; Liu, X.; Wei, L.; Wu, K.; Fu, Q. A self-reinforcing and self-healing elastomer with high strength, unprecedented toughness and room-temperature reparability. *Mater. Horiz.* **2021**, *8*, 267–275.

(29) Liu, S.; Fan, X.; He, C. Improving the fracture toughness of epoxy with nanosilica-rubber core-shell nanoparticles. *Compos. Sci. Technol.* **2016**, *125*, 132–140.

(30) Yu, X.; Wang, Y.; Zhang, H.; Fan, X.; Liu, T. Ultrastretchable and Stable Conductive Elastomer Based on Micro-Ionicgel for Wide-Working-Range Sensors. *ACS Appl. Mater. Interfaces* **2021**, *13*, 53091–53098.

(31) Jia, X.; Li, Y.; Cheng, Q.; Zhang, S.; Zhang, B. Preparation and properties of poly(vinyl alcohol)/silica nanocomposites derived from copolymerization of vinyl silica nanoparticles and vinyl acetate. *Eur. Polym. J.* **2007**, *43*, 1123–1131.

(32) Mostafa, H. Y.; Hussain, A. I.; El-Masry, A. M.; Maher, A. Novel Core-Shell of Polymethyl Methacrylate/butyl Acrylate/vinyl Silica Nanocomposite Particles through Seed Emulsion Polymerization. *Polym.-Plast. Technol. Eng.* **2017**, *56*, 411–420.

(33) Mozhdehi, D.; Ayala, S.; Cromwell, O. R.; Guan, Z. Self-Healing Multiphase Polymers via Dynamic Metal-Ligand Interactions. *J. Am. Chem. Soc.* **2014**, *136*, 16128–16131.

(34) Ji, S.; Cao, W.; Yu, Y.; Xu, H. Visible-Light-Induced Self-Healing Diselenide-Containing Polyurethane Elastomer. *Adv. Mater.* **2015**, *27*, 7740–7745.

(35) Deng, J.; Kuang, X.; Liu, R.; Ding, W.; Wang, A. C.; Lai, Y.-C.; Dong, K.; Wen, Z.; Wang, Y.; Wang, L.; Qi, H. J.; Zhang, T.; Wang, Z. L. Vitrimer Elastomer-Based Jigsaw Puzzle-Like Healable Triboelectric Nanogenerator for Self-Powered Wearable Electronics. *Adv. Mater.* **2018**, *30*, No. 1705918.

(36) Xie, R.; Mukherjee, S.; Levi Adam, E.; Reynolds Veronica, G.; Wang, H.; Chabinyc Michael, L.; Bates Christopher, M. Room temperature 3D printing of super-soft and solvent-free elastomers. *Sci. Adv.* **2020**, *6*, No. eabc6900.

(37) Yang, Y.; Wang, X.; Yang, F.; Shen, H.; Wu, D. A Universal Soaking Strategy to Convert Composite Hydrogels into Extremely Tough and Rapidly Recoverable Double-Network Hydrogels. *Adv. Mater.* **2016**, *28*, 7178–7184.

(38) Lei, Z.; Wang, Q.; Sun, S.; Zhu, W.; Wu, P. A Bioinspired Mineral Hydrogel as a Self-Healable, Mechanically Adaptable Ionic Skin for Highly Sensitive Pressure Sensing. *Adv. Mater.* **2017**, *29*, No. 1700321.

(39) Wang, Z.; Pan, Q. An Omni-Healable Supercapacitor Integrated in Dynamically Cross-Linked Polymer Networks. *Adv. Funct. Mater.* **2017**, *27*, No. 1700690.

(40) Mo, F.; Chen, Z.; Liang, G.; Wang, D.; Zhao, Y.; Li, H.; Dong, B.; Zhi, C. Zwitterionic Sulfobetaine Hydrogel Electrolyte Building Separated Positive/Negative Ion Migration Channels for Aqueous Zn-MnO<sub>2</sub> Batteries with Superior Rate Capabilities. *Adv. Energy Mater.* **2020**, *10*, No. 2000035.

(41) Li, L.; Zhang, Y.; Lu, H.; Wang, Y.; Xu, J.; Zhu, J.; Zhang, C.; Liu, T. Cryopolymerization enables anisotropic polyaniline hybrid hydrogels with superelasticity and highly deformation-tolerant electrochemical energy storage. *Nat. Commun.* **2020**, *11*, 62.

(42) Hua, Q.; Sun, J.; Liu, H.; Bao, R.; Yu, R.; Zhai, J.; Pan, C.; Wang, Z. L. Skin-inspired highly stretchable and conformable matrix networks for multifunctional sensing. *Nat. Commun.* **2018**, *9*, 244.

(43) Trung, T. Q.; Ramasundaram, S.; Hwang, B.-U.; Lee, N.-E. An All-Elastomeric Transparent and Stretchable Temperature Sensor for

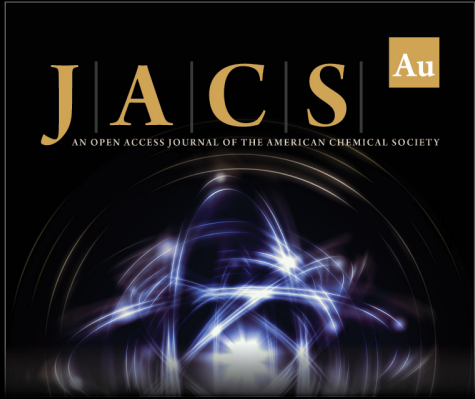
Body-Attachable Wearable Electronics. *Adv. Mater.* **2016**, *28*, 502–509.

(44) Honda, W.; Harada, S.; Ishida, S.; Arie, T.; Akita, S.; Takei, K. High-Performance, Mechanically Flexible, and Vertically Integrated 3D Carbon Nanotube and InGaZnO Complementary Circuits with a Temperature Sensor. *Adv. Mater.* **2015**, *27*, 4674–4680.

(45) He, W.; Li, G.; Zhang, S.; Wei, Y.; Wang, J.; Li, Q.; Zhang, X. Polypyrrole/Silver Coaxial Nanowire Aero-Sponges for Temperature-Independent Stress Sensing and Stress-Triggered Joule Heating. *ACS Nano* **2015**, *9*, 4244–4251.

(46) An, B. W.; Heo, S.; Ji, S.; Bien, F.; Park, J.-U. Transparent and flexible fingerprint sensor array with multiplexed detection of tactile pressure and skin temperature. *Nat. Commun.* **2018**, *9*, 2458.

(47) Bang, J.; Lee, W. S.; Park, B.; Joh, H.; Woo, H. K.; Jeon, S.; Ahn, J.; Jeong, C.; Kim, T.-I.; Oh, S. J. Highly Sensitive Temperature Sensor: Ligand-Treated Ag Nanocrystal Thin Films on PDMS with Thermal Expansion Strategy. *Adv. Funct. Mater.* **2019**, *29*, No. 1903047.



**JACS** Au  
AN OPEN ACCESS JOURNAL OF THE AMERICAN CHEMICAL SOCIETY

 Editor-in-Chief  
**Prof. Christopher W. Jones**  
Georgia Institute of Technology, USA

**Open for Submissions** 

pubs.acs.org/jacsau  ACS Publications  
Most Trusted. Most Cited. Most Read.